

Effect of the Phase Composition and Local Crystal Structure on the Transport Properties of the $\text{ZrO}_2\text{--Y}_2\text{O}_3$ and $\text{ZrO}_2\text{--Gd}_2\text{O}_3$ Solid Solutions

E. A. Agarkova^a, M. A. Borik^b, V. T. Bublik^c, T. V. Volkova^d, A. V. Kulebyakin^b, I. E. Kuritsyna^a,
N. A. Larina^d, E. E. Lomonova^b, F. O. Milovich^c, V. A. Myzina^b,
P. A. Ryabochkina^d, and N. Yu. Tabachkova^{b, c, *}

^aInstitute of Solid State Physics, Russian Academy of Sciences, Moscow oblast, Chernogolovka, 142432 Russia

^bProkhorov General Physics Institute, Russian Academy of Sciences, Moscow, 119991 Russia

^cNational University of Science and Technology MISIS, Moscow, 119049 Russia

^dOgarev National Research Mordovia State University, Republic of Mordovia, Saransk, 430005 Russia

*e-mail: ntabachkova@gmail.com

Received January 18, 2019

Abstract—The results of investigating the crystal structure, ionic conductivity, and local structure of the $(\text{ZrO}_2)_{1-x}(\text{Gd}_2\text{O}_3)_x$ and $(\text{ZrO}_2)_{1-x}(\text{Y}_2\text{O}_3)_x$ ($x = 0.04, 0.08, 0.10, 0.12$, and 0.14) solid solutions are reported. The crystals are grown by directional crystallization of the melt in a cold container. The phase composition of the crystals is investigated by X-ray diffractometry and transmission electron microscopy. The transport characteristics are studied by impedance spectroscopy in the temperature range of 400 to 900°C. The local crystal structure is examined by optical spectroscopy. Eu^{3+} ions were used as a spectroscopic probe. The study of the local structure of the $\text{ZrO}_2\text{--Y}_2\text{O}_3$ and $\text{ZrO}_2\text{--Gd}_2\text{O}_3$ solid solutions revealed the features in the formation of optical centers, which reflect the character of localization of oxygen vacancies in the crystal lattice depending on the stabilizing oxide concentration. It is established that the local crystal environment of Eu^{3+} ions in the $(\text{ZrO}_2)_{1-x}(\text{Y}_2\text{O}_3)_x$ and $(\text{ZrO}_2)_{1-x}(\text{Gd}_2\text{O}_3)_x$ solid solutions is determined by the stabilizing oxide concentration and is practically independent of the stabilizing oxide type (Y_2O_3 or Gd_2O_3). The maximum conductivity at a temperature of 900°C is observed in the crystals with 10 mol % of Gd_2O_3 and 8 mol % of Y_2O_3 . These compositions correspond to the t' phase and are close to the interface between the cubic and tetragonal phase regions. It is found that in the $\text{ZrO}_2\text{--Y}_2\text{O}_3$ system the highly symmetric phase is stabilized at a lower stabilizing oxide concentration than in the $\text{ZrO}_2\text{--Gd}_2\text{O}_3$ system. The analysis of the data obtained makes it possible to conclude that, in this composition range, the concentration dependence of the ionic conductivity is mainly affected by the phase composition rather than the character of the localization of oxygen vacancies in the crystal lattice.

Keywords: zirconia, $\text{ZrO}_2\text{--Y}_2\text{O}_3$, $\text{ZrO}_2\text{--Gd}_2\text{O}_3$, crystal growth, ion conductivity, local structure, phase analysis

DOI: 10.1134/S1063739719080043

INTRODUCTION

The zirconium dioxide-based materials have a high degree of ionic conductivity at high temperatures and are therefore widely used as solid electrolytes in solid oxide fuel cells [1–3]. The oxygen-ion conductivity of the zirconium dioxide-based solid solutions is caused by oxygen vacancies in their anion sublattice, which are formed due to the necessity for charge compensation upon heterovalent substitution of stabilizing oxide cations with valence 3+ or 2+ for Zr^{4+} ions [4]. The ionic conductivity of the zirconium dioxide-based solid solutions depends on the type and concentration of the stabilizing oxide and is determined by a number of factors, but primarily by the phase composition and

the concentration and mobility of the oxygen vacancies involved in the charge transport.

The dependence of the conductivity on the type and concentration of the stabilizing oxide was studied in detail in [5]. It was shown that an increase in the ionic radius of the stabilizing cation leads to a decrease in the maximum ionic conductivity. In this case, the stabilizing oxide concentration corresponding to the maximum conductivity decreases with the increasing ionic radius of the stabilizing cation [6].

The effect of the interaction of oxygen vacancies with the stabilizing oxide cations on the transport properties of the oxides with the fluorite structure was thoroughly investigated in [6]. The presence of different complexes for the zirconium oxide-based materi-

Table 1. Compositions, designations, and densities of the grown crystals

ZrO ₂ –Y ₂ O ₃			ZrO ₂ –Gd ₂ O ₃		
crystal composition	designation	density, g/cm ³	crystal composition	designation	density, g/cm ³
(ZrO ₂) _{0.96} (Y ₂ O ₃) _{0.04}	4YSZ	6.020(2)	(ZrO ₂) _{0.96} (Gd ₂ O ₃) _{0.04}	4GdSZ	6.251(2)
(ZrO ₂) _{0.92} (Y ₂ O ₃) _{0.08}	8YSZ	6.010(2)	(ZrO ₂) _{0.92} (Gd ₂ O ₃) _{0.08}	8GdSZ	6.394(2)
(ZrO ₂) _{0.90} (Y ₂ O ₃) _{0.10}	10YSZ	5.950(2)	(ZrO ₂) _{0.90} (Gd ₂ O ₃) _{0.10}	10GdSZ	6.481(2)
(ZrO ₂) _{0.88} (Y ₂ O ₃) _{0.12}	12YSZ	5.928(2)	(ZrO ₂) _{0.88} (Gd ₂ O ₃) _{0.12}	12GdSZ	6.533(2)
(ZrO ₂) _{0.86} (Y ₂ O ₃) _{0.14}	14YSZ	5.882(2)	(ZrO ₂) _{0.86} (Gd ₂ O ₃) _{0.14}	14GdSZ	6.586(2)

als was discussed in [7–13]. The type of forming complexes can be characterized by the position of oxygen vacancies relative to the zirconium and dopant cations, i.e., the local structure of the crystal lattice.

To date, there have been a large number of works on the computer modeling of local structural defects and their interaction in solid oxide electrolytes using different approaches [10–15]. One of the experimental methods for studying the local crystal structure is optical spectroscopy. This method with the Eu³⁺ ion as a spectroscopic probe is widely used for studying the local structure of the crystals, including the zirconium dioxide-based solid solutions [9, 16–18].

The aim of this study was to establish the correlation between the transport characteristics, structure, and phase composition in the ZrO₂–Y₂O₃ and ZrO₂–Gd₂O₃ crystals depending on the type and composition of a stabilizing oxide.

EXPERIMENTAL

The (ZrO₂)_{1–x}(Y₂O₃)_x and (ZrO₂)_{1–x}(Gd₂O₃)_x ($x = 0.04, 0.08, 0.10, 0.12, \text{ and } 0.14$) solid solution crystals were grown by directional crystallization from melt in a cold container 130 mm in diameter at a growth rate of 10 mm/h [19]. All the solid solutions were additionally doped with 0.1 mol % of Eu₂O₃. The Eu³⁺ ions were used as a spectroscopic probe for studying the local crystal structure by optical spectroscopy. The crystals were grown on a Kristall-407 facility at a frequency of 5.28 MHz and an output power of 60 kW. The load mass was 6 kg. The charge was prepared from the ZrO₂, Y₂O₃, Gd₂O₃, and Eu₂O₃ powders with purity of at least 99.99%.

The phase composition of the crystals was determined by X-ray diffractometry using a Bruker D8 instrument. The phase analysis was made on the plates cut from the crystals perpendicular to the $\langle 100 \rangle$ direction. The crystal structure was studied by transmission electron microscopy using a JEM 2100 microscope at an accelerating voltage of 200 kV. The samples were thinned by ion etching using a PIPS II apparatus.

The transport characteristics of the crystals were studied on a Solartron SI 1260 analyzer in the tem-

perature range of 400 to 900°C with a step of 50°C at frequencies of 1 Hz to 5 MHz. The measurements were taken on 7×7 mm²-crystal plates 0.5 mm thick with symmetric platinum electrodes. Before the measurements, the plates were coated with the platinum paste and annealed in air at a temperature of 950°C for 1 h. The amplitude of the ac signal applied to the sample was 24 mV. A detailed analysis of the frequency spectrum of the impedance was performed using the ZView program. The resistance of the electrolytes was calculated from the obtained impedance spectra and, then, the electrical conductivity of the crystals was calculated.

The luminescence spectra were recorded at temperatures of 300 and 77 K using a Horiba FHR 1000 spectrometer. A Hamamatsu R928 PMT was used as the radiation detector. The luminescence was excited to the ⁵D₁ level by the second-harmonic radiation of YVO₄: Nd lasers with wavelength $\lambda_{\text{exc}} = 532$ nm. The luminescence was excited to the ⁵L₆ level of Eu³⁺ ions using the third harmonic of the LiYF₄: Nd laser with a wavelength of 351 nm.

RESULTS AND DISCUSSION

The compositions of the grown crystals, the corresponding designations, and the crystal densities are given in Table 1.

The gadolinium oxide-stabilized crystals did not fundamentally differ in shape, color, and size from the yttrium oxide-stabilized crystals. All the crystals had a columnar shape typical of the growth technique used. In the investigated composition range, homogeneous transparent single crystals were obtained at $x = 0.08$ – 0.14 for the (ZrO₂)_{1–x}(Y₂O₃)_x solid solutions and at $x = 0.10$ – 0.14 for the (ZrO₂)_{1–x}(Gd₂O₃)_x solid solutions. In contrast to the homogeneous transparent 8YSZ single crystals, the 8GdSZ crystals were semi-transparent, but without visible defects in the bulk of the ingot. The 4YSZ crystals were white and opaque, similar to the 4GdSZ crystals.

As the Y₂O₃ concentration in the ZrO₂–Y₂O₃-based solid solutions grows, the crystal density decreases, since the density of Y₂O₃ (4.850 g/cm³) is lower than the

Table 2. Phase composition and parameters of the $(\text{ZrO}_2)_{1-x}(\text{Y}_2\text{O}_3)_x$ and $(\text{ZrO}_2)_{1-x}(\text{Gd}_2\text{O}_3)_x$ crystal structure

$\text{ZrO}_2\text{-Y}_2\text{O}_3$			$\text{ZrO}_2\text{-Gd}_2\text{O}_3$		
sample	phase*	lattice parameters, nm	sample	phase*	lattice parameters, nm
4YSZ	<i>t</i>	$a = 0.3606(1), c = 0.5169(1)$	4GdSZ	<i>t</i>	$a = 0.3609(1), c = 0.5182(1)$
	<i>t'</i>	$a = 0.3626(1), c = 0.5147(2)$		<i>t'</i>	$a = 0.3636(1), c = 0.5155(2)$
8YSZ	<i>c</i>	$a = 0.5138(1)$	8GdSZ	<i>t'</i>	$a = 0.3641(1), c = 0.5155(1)$
10YSZ	<i>c</i>	$a = 0.5144(1)$	10GdSZ	<i>c</i>	$a = 0.5159(1)$
12YSZ	<i>c</i>	$a = 0.5148(1)$	12GdSZ	<i>c</i>	$a = 0.5167(1)$
14YSZ	<i>c</i>	$a = 0.5153(1)$	14GdSZ	<i>c</i>	$a = 0.5175(1)$

* *t* is the tetragonal ZrO_2 modification and *c* is the cubic ZrO_2 modification.

density of ZrO_2 (5.68 g/cm³). The density of Gd_2O_3 (7.407 g/cm³) is higher than the density of ZrO_2 ; therefore, the density of the $\text{ZrO}_2\text{-Gd}_2\text{O}_3$ crystals increases with the Gd_2O_3 concentration.

Table 2 gives the phase composition and crystal lattice parameters for the Y_2O_3 - and Gd_2O_3 -stabilized ZrO_2 crystals.

The 4YSZ and 4GdSZ crystals contained two tetragonal zirconium dioxide phases *t* and *t'* with different degrees of tetragonality. The presence of these two phases is caused by the decomposition of the high-temperature cubic solid solution into two metastable tetragonal phases. At the transition from the single-phase cubic region to the double-phase (*c* + *t*) region of the equilibrium phase diagram of the $\text{ZrO}_2\text{-Y}_2\text{O}_3$ system, $\text{ZrO}_2\text{-Gd}_2\text{O}_3$ does not decompose into stable phases. At some supercooling critical for a given composition, a first-order phase transition occurs, which is accompanied by the redistribution of the stabilizing impurity and formation of two metastable tetragonal phases with the compositions lying inside the double-phase region near the equilibrium boundaries. At the stabilizing oxide concentration of 8 mol %, the phase composition of the crystals depended on the stabilizing oxide type; the 8GdSZ crystals had a tetragonal structure; and the 8YSZ crystals, a cubic structure. At a concentration above 8 mol % of Y_2O_3 and 10 mol % of Gd_2O_3 , the crystals were single-phase with a fluorite structure. In the cubic solid solutions, the crystal lattice parameter increased almost linearly with the increasing stabilizing oxide concentration. At the comparable concentrations, the lattice parameter of the Y_2O_3 -stabilized cubic crystals was smaller than that of the Gd_2O_3 -stabilized crystals. It should be noted that the cubic phase in the crystals co-doped with Y_2O_3 stabilizes at a lower Y_2O_3 concentration in the solid solution than in the crystals co-doped with Gd_2O_3 . This can be related to the dependence of the mechanism of stabilization of the high-temperature phase on the type of a stabilizing impurity. In the $\text{ZrO}_2\text{-Y}_2\text{O}_3$ binary systems, a decrease in the ionic

radius reduces the temperature of the transition from the high-temperature cubic phase to the low-temperature tetragonal phase [20]. This will lead to the preservation of the high-temperature cubic phase at room temperature at a lower stabilizing oxide concentration.

The transmission microscopy study of the crystals showed that the 4YSZ and 4GdSZ crystal structure consisted of twins (Fig. 1). The twinning plane is the {110} plane. Coarse twins were observed in the 4GdSZ crystals (Fig. 1a), which, in turn, consisted of smaller twins; i.e., each of the twins contained a twin of the next order. In the 4YSZ crystals, the twin structure was more uniform and the twins were smaller (Fig. 1b).

The difference in morphology and dispersion of the twin structure in the 4YSZ and 4GdSZ crystals may be due to the fact that, according to the $\text{ZrO}_2\text{-Y}_2\text{O}_3$ and $\text{ZrO}_2\text{-Gd}_2\text{O}_3$ phase diagrams, the transition from the single-phase cubic to the double-phase region upon cooling the crystals stabilized by 4 mol % of Y_2O_3 occurs at lower temperatures than in the crystals stabilized with 4 mol % Gd_2O_3 . The different temperatures of the phase transitions can affect the morphology and twin size. In the 4YSZ crystals, twinning occurs simultaneously and is localized in small volumes, in contrast to the 4GdSZ samples, where twinning occurs first in coarser domains, which, in turn, also undergo twinning.

Figure 2 shows the 8GdSZ and 8YSZ crystal structures. In the tetragonal 8GdSZ crystals, a finely dispersed twin structure was observed (Fig. 2a), while in the 8YSZ crystals there were no twins, which is typical of single-phase cubic single crystals (Fig. 2b). However, in the diffraction patterns of the 8YSZ crystals, there were reflections forbidden for the cubic lattice and allowed for the tetragonal structure. The presence of 110 and 112 reflections is indicative of the ordered displacement of oxygen atoms and, consequently, a violation of the symmetry which is characteristic of the space group *Fm3m*. These data show that the 8YSZ crystals are tetragonal (*t''* phase) and not cubic, as follows from the X-ray diffractometry data. The existence of the *t''* phase was found in [21]. This phase was

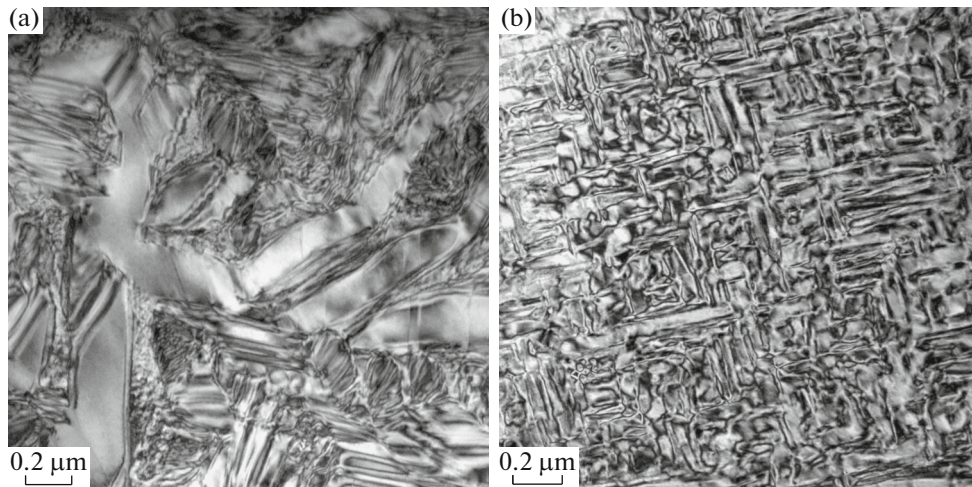


Fig. 1. Image of twinning in (a) the 4GdSZ and (b) 4YSZ crystals.

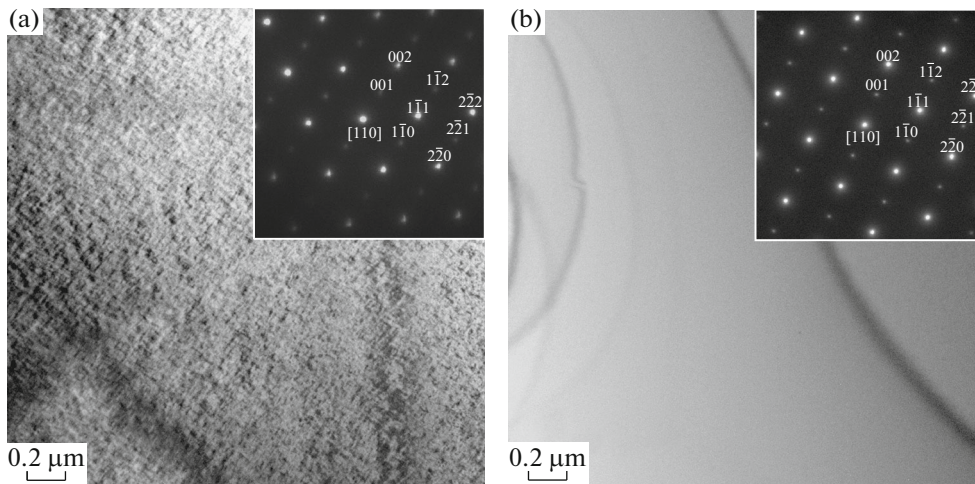


Fig. 2. Image of (a) the 8GdSZ and (b) 8YSZ crystal structure. Inset: electron diffraction patterns.

described as having a tetragonality degree of $c/a = 1$, but with sp. gr. $P4_2/nmc$ due to the displacement of oxygen atoms in the anion sublattice.

The analysis of the electron diffraction patterns of the crystals belonging, according to the XRD data, to the cubic phase showed that the 8YSZ, 10YSZ, 10GdSZ, and 12GdSZ crystals belong to the t'' phase. In the investigated composition range, only the 12YSZ, 14YSZ, and 14GdSZ crystals had a fluorite cubic structure.

The features of the local structure of the ZrO_2 – Y_2O_3 and ZrO_2 – Gd_2O_3 crystals formed with regard to the oxygen vacancies were studied by optical spectroscopy. Figures 3 and 4 show the luminescence spectra of the $(ZrO_2)_{1-x}(Y_2O_3)_x$ and $(ZrO_2)_{1-x}(Gd_2O_3)_x$ ($x = 0.04, 0.08, 0.10, 0.12, \text{ and } 0.14$) crystals doped with Eu^{3+} ions caused by the transitions ${}^5D_0 \rightarrow {}^7F_0$, ${}^5D_0 \rightarrow {}^7F_1$,

and ${}^5D_0 \rightarrow {}^7F_2$ of Eu^{3+} ions upon excitation to the 5D_1 level ($\lambda_{exc} = 532 \text{ nm}$) at temperatures of 300 and 77 K.

A comparison of the luminescence spectra of the ZrO_2 – Gd_2O_3 crystals showed that their shape and line positions are similar to those of the luminescence spectra of the ZrO_2 – Y_2O_3 crystals at similar stabilizing oxide concentrations.

Since the energy gap between the 7F_0 and 7F_1 levels of Eu^{3+} ions estimated from the luminescence spectra for the Gd_2O_3 (Y_2O_3)-stabilized zirconium crystals is $\sim 200 \text{ cm}^{-1}$, the 7F_1 level at a temperature of $T = 77 \text{ K}$ appears unoccupied. Consequently, the excitation of the luminescence spectra for the ZrO_2 – Gd_2O_3 and ZrO_2 – Y_2O_3 crystals at $T = 300 \text{ K}$ occurs via both the ${}^7F_0 \rightarrow {}^5D_1$ and ${}^7F_1 \rightarrow {}^5D_1$ transition and, at $T = 77 \text{ K}$, the luminescence is excited via the transition ${}^7F_0 \rightarrow {}^5D_1$ of Eu^{3+} ions.

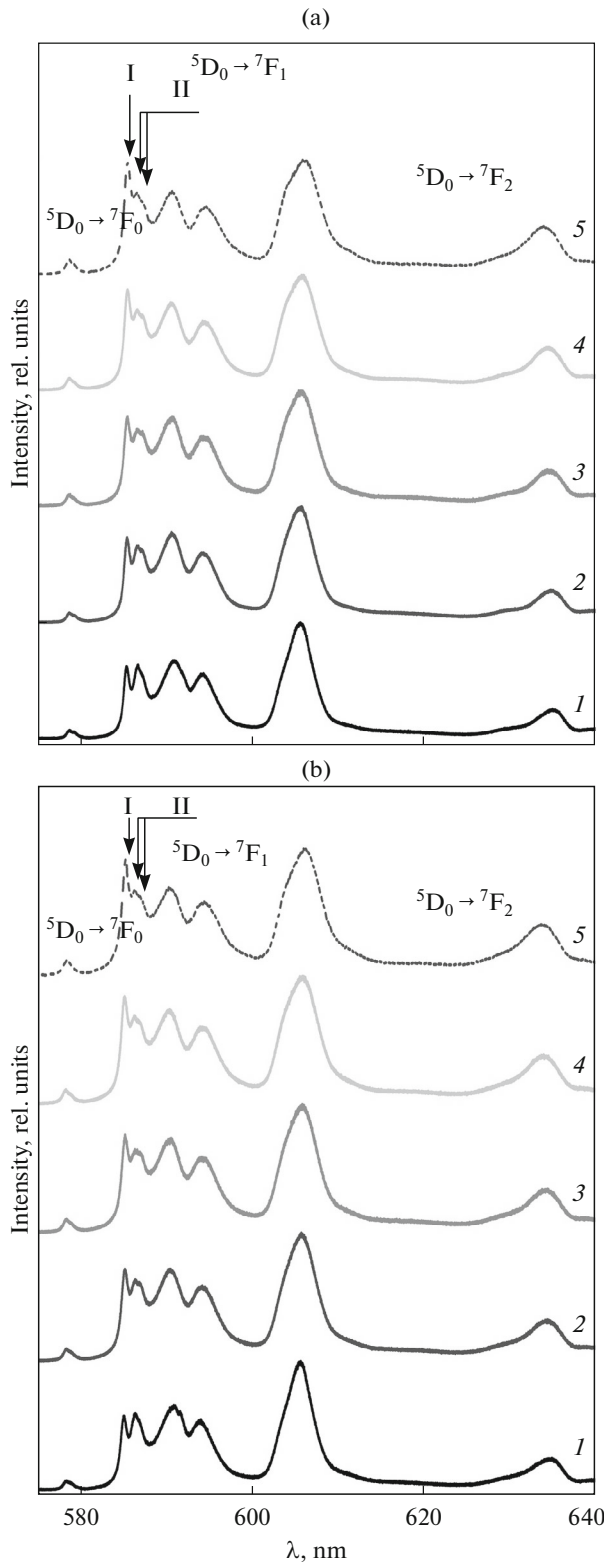


Fig. 3. Luminescence spectra for (a) the $(\text{ZrO}_2)_{1-x}(\text{Y}_2\text{O}_3)_x$ and (b) $(\text{ZrO}_2)_{1-x}(\text{Gd}_2\text{O}_3)_x$ crystals doped with Eu^{3+} ions caused by the transitions ${}^5\text{D}_0 \rightarrow {}^7\text{F}_0$, ${}^5\text{D}_0 \rightarrow {}^7\text{F}_1$, and ${}^5\text{D}_0 \rightarrow {}^7\text{F}_2$ of Eu^{3+} ions upon excitation to the level ${}^5\text{D}_1$ ($\lambda_{\text{exc}} = 532$ nm) at $T = 300$ K: (1) $x = 0.04$, (2) 0.08, (3) 0.10, (4) 0.12, and (5) 0.14.

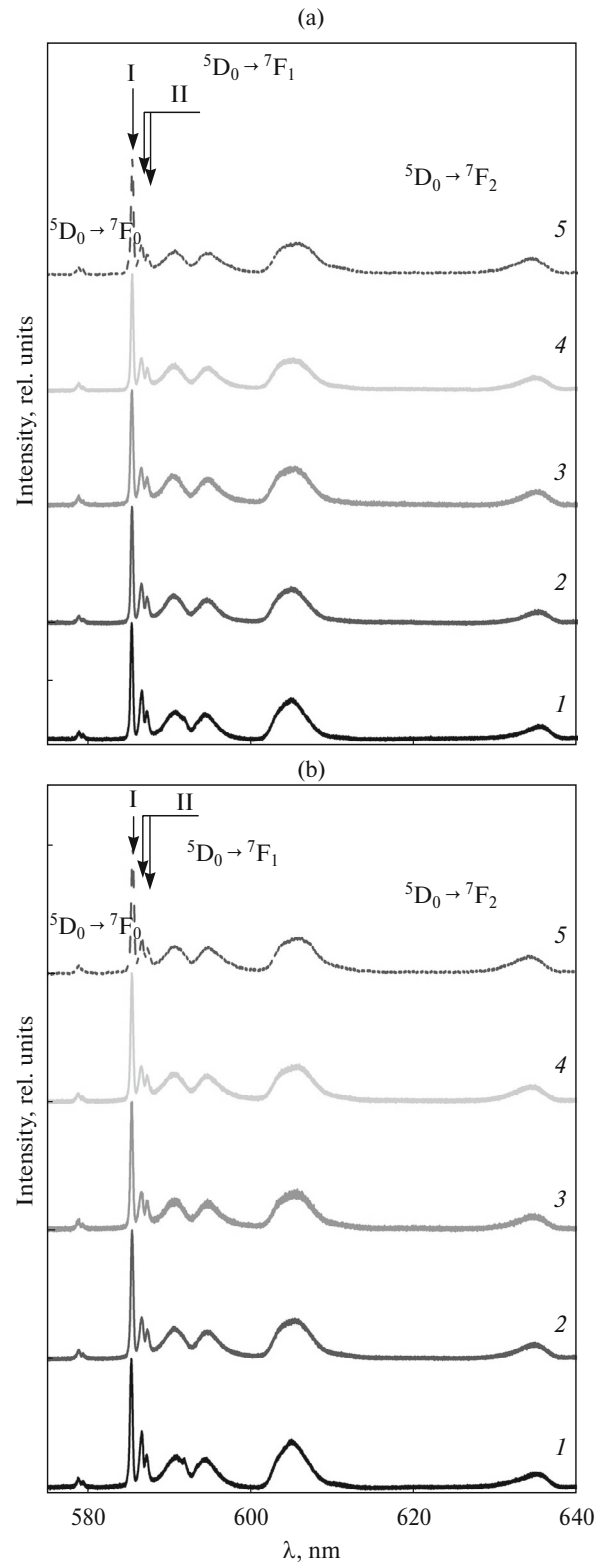


Fig. 4. Luminescence spectra for (a) the $(\text{ZrO}_2)_{1-x}(\text{Y}_2\text{O}_3)_x$ and (b) $(\text{ZrO}_2)_{1-x}(\text{Gd}_2\text{O}_3)_x$ crystals doped with Eu^{3+} ions caused by the transitions ${}^5\text{D}_0 \rightarrow {}^7\text{F}_0$, ${}^5\text{D}_0 \rightarrow {}^7\text{F}_1$, and ${}^5\text{D}_0 \rightarrow {}^7\text{F}_2$ of Eu^{3+} ions upon excitation to the level ${}^5\text{D}_1$ ($\lambda_{\text{exc}} = 532$ nm) at $T = 77$ K: (1) 0.04, (2) 0.08, (3) 0.10, (4) 0.12, and (5) 0.14.

Table 3. Ratio between the integral intensities of the spectral lines for the transitions ${}^5D_0 \rightarrow {}^7F_2$ and ${}^5D_0 \rightarrow {}^7F_1$ estimated from the luminescence spectra with $\lambda_{\text{exc}} = 532$ nm at temperatures of 300 and 77 K

Sample	Ratio between the integral intensities for the transitions ${}^5D_0 \rightarrow {}^7F_2$ and ${}^5D_0 \rightarrow {}^7F_1$		Sample	Ratio between the integral intensities for the transitions ${}^5D_0 \rightarrow {}^7F_2$ and ${}^5D_0 \rightarrow {}^7F_1$	
	$T = 300$ K	$T = 77$ K		$T = 300$ K	$T = 77$ K
4GdSZ	1.1	0.9	4YSZ	1.1	0.9
8GdSZ	1.2	1.0	8YSZ	1.1	0.9
10GdSZ	1.2	1.0	10YSZ	1.1	1.0
12GdSZ	1.2	1.0	12YSZ	1.3	1.1
14GdSZ	1.3	1.1	14YSZ	1.3	1.2

In the luminescence spectra of the crystals with the $\text{Gd}_2\text{O}_3(\text{Y}_2\text{O}_3)$ concentrations from 4 to 14 mol % detected at both $T = 300$ K and $T = 77$ K for the transition ${}^5D_0 \rightarrow {}^7F_1$, the relative intensity of the line with the maximum at 585.5 nm increases relative to the lines at 586.6 and 587.3 nm.

Taking into account the features of the variation in the luminescence spectra recorded upon excitation by the radiation with $\lambda_{\text{exc}} = 532$ nm at $T = 300$ and 77 K, for the transitions ${}^5D_0 \rightarrow {}^7F_1$ and ${}^5D_0 \rightarrow {}^7F_2$ of Eu^{3+} ions in the ZrO_2 crystals with different contents of the stabilizing oxide, we identified the types of optical centers of Eu^{3+} ions in the $\text{ZrO}_2\text{-Y}_2\text{O}_3$ and $\text{ZrO}_2\text{-Gd}_2\text{O}_3$ crystals.

The line with the maximum at 585.5 nm belongs to the type-I optical center. The center of this type corresponds to the Eu^{3+} ion with one oxygen vacancy in the nearest environment and is located in the oxygen seven-vortex surrounding. The point symmetry of this optical center of the Eu^{3+} ion should be trigonal (C_{3v}). In this case, the 7F_1 level of the Eu^{3+} ion should be split into two Stark components. Additional distortions lead to the symmetry lowering; then, the 7F_1 level of the Eu^{3+} ion will be split into three Stark components [16]. The luminescence spectra for the $\text{ZrO}_2\text{-Gd}_2\text{O}_3$ and $\text{ZrO}_2\text{-Y}_2\text{O}_3$ crystals presented in Figs. 3 and 4 are the superposition of the spectra for different optical centers of Eu^{3+} ions with the nonuniformly broadened spectral lines. Therefore, it is impossible to unambiguously determine the number of Stark components corresponding to the 5D_1 level of the type-I Eu^{3+} optical center.

The lines with the maxima at 586.6 and 587.3 nm in the luminescence spectra at $T = 300$ K for the $\text{ZrO}_2\text{-Y}_2\text{O}_3$ and $\text{ZrO}_2\text{-Gd}_2\text{O}_3$ crystals, as well as the lines with the maxima at 586.7 and 587.3 nm in the luminescence spectra at $T = 77$ K, are attributed to the type-II optical centers of Eu^{3+} ions. In the centers of this type, there are no oxygen vacancies in the first coordination sphere, but they are contained in the second one. The local symmetry of such centers corre-

sponds to C_1 . According to the data reported in [16], the splitting of the 7F_1 level by the crystal field for these Eu^{3+} centers is weaker than for the type-I spectra.

The rare-earth ions with the characteristic super-sensitive transitions between their energy levels can serve as spectroscopy probes for detecting the features of the local crystal structure [22, 23].

In [24, 25], it was shown by the example of intensities of the supersensitive optical transitions between the energy levels of rare-earth ions in garnet crystals that the intensity of the super-sensitive transitions of rare-earth ions in them significantly increase if the point symmetry of a rare-earth ion corresponds to C_{2v} , C_2 , and C_1 .

For Eu^{3+} ions, the transition ${}^5D_0 \rightarrow {}^7F_2$ is supersensitive. The intensity of this transition will significantly depend on the crystal environment. At the same time, the intensity of the magnetic-dipole transition ${}^5D_0 \rightarrow {}^7F_1$ of the Eu^{3+} ion is insensitive to the crystal environment. Therefore, an increase in the ratio between the intensities of the transitions ${}^5D_0 \rightarrow {}^7F_2$ and ${}^5D_0 \rightarrow {}^7F_1$ of Eu^{3+} ions in the investigated crystals serve as evidence for the increase in the relative fraction of lower-symmetry centers in them.

The ratios between the integral intensities of the lines for the supersensitive transition ${}^5D_0 \rightarrow {}^7F_2$ and magnetic-dipole transition ${}^5D_0 \rightarrow {}^7F_1$ of Eu^{3+} ions obtained from the luminescence spectra (Figs. 3, 4) are given in Table 3.

It follows from the data given in Table 3 that the ratios between the integral intensities of the spectral lines for the transitions ${}^5D_0 \rightarrow {}^7F_2$ and ${}^5D_0 \rightarrow {}^7F_1$ of Eu^{3+} ions increase with the concentration of the stabilizing Gd_2O_3 (Y_2O_3) oxide due to the increase in the relative fraction of the low-symmetry Eu^{3+} optical centers.

Having generalized the features of the local structure of the $\text{ZrO}_2\text{-Gd}_2\text{O}_3$ and $\text{ZrO}_2\text{-Y}_2\text{O}_3$ crystals, we may conclude that the local crystal environment of Eu^{3+} ions in the $(\text{ZrO}_2)_{1-x}(\text{Y}_2\text{O}_3)_x$ and $(\text{ZrO}_2)_{1-x}(\text{Gd}_2\text{O}_3)_x$ ($x = 0.04, 0.08, 0.10, 0.12, \text{ and } 0.14$) solid solutions

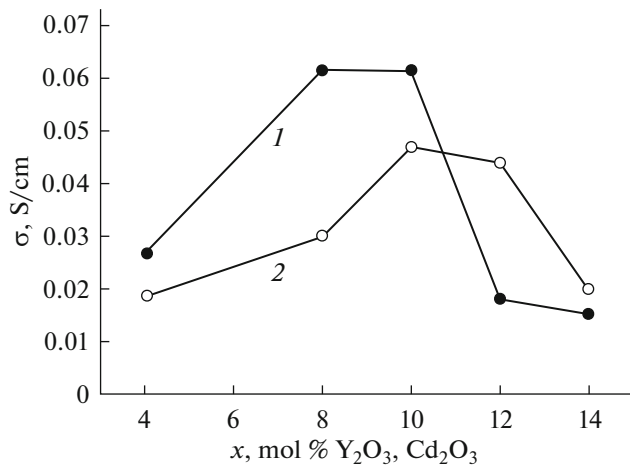


Fig. 5. Crystal conductivity σ at a temperature of 1173 K: (1) $(\text{ZrO}_2)_{1-x}(\text{Y}_2\text{O}_3)_x$ and (2) $(\text{ZrO}_2)_{1-x}(\text{Gd}_2\text{O}_3)_x$.

formed with oxygen vacancies involved is determined by the stabilizing oxide concentration and is almost independent of the oxide type (Y_2O_3 or Gd_2O_3). The relative fraction of the positions of Eu^{3+} (Y^{3+} , Gd^{3+}) ions with the oxygen vacancies in the nearest coordination sphere increases at the stabilizing (Y_2O_3 , Gd_2O_3) oxide concentrations above 8 mol %.

Figure 5 shows the dependences of the conductivity of the $\text{ZrO}_2\text{-Gd}_2\text{O}_3$ and $\text{ZrO}_2\text{-Y}_2\text{O}_3$ crystals at a temperature of 1173 K. It can be seen that the change in the conductivity with increasing stabilizing oxide concentration is analogous for Y_2O_3 and Gd_2O_3 . However, the maximum conductivity of the $\text{ZrO}_2\text{-Gd}_2\text{O}_3$ solid solution shifts toward higher concentrations relative to the maximum conductivity of the $\text{ZrO}_2\text{-Y}_2\text{O}_3$ solid solutions. For instance, the maximum conductivity of the $\text{ZrO}_2\text{-Y}_2\text{O}_3$ solid solution was observed at 8–10 mol % of Y_2O_3 , while for the $\text{ZrO}_2\text{-Gd}_2\text{O}_3$ solid solution, this concentration was 10–12 mol % of Gd_2O_3 . Note that the maximum conductivity in the $\text{ZrO}_2\text{-Y}_2\text{O}_3$ system was higher than that in the $\text{ZrO}_2\text{-Gd}_2\text{O}_3$ system. The growth of the Y_2O_3 concentration above 10 mol % and the Gd_2O_3 concentration above 12 mol % led to a decrease in the conductivity.

The conductivities of the tetragonal 4GdSZ and 4YSZ crystals at 1173 K were similar. As the Gd_2O_3 concentration increases from 4 to 10 mol %, the conductivity of the crystals grows. The 10GdSZ crystals with the t'' phase have the maximum conductivity. In the $\text{ZrO}_2\text{-Y}_2\text{O}_3$ system, the occurrence of the t'' phase was observed in the crystals with the lower concentration of the stabilizing oxide (8YSZ) and these crystals also have the maximum conductivity. At the transition from the t'' to the cubic phase, the ionic conductivity decreases with the increasing Gd_2O_3 or Y_2O_3 concentration.

CONCLUSIONS

The crystals of the $(\text{ZrO}_2)_{1-x}(\text{Gd}_2\text{O}_3)_x$ and $(\text{ZrO}_2)_{1-x}(\text{Y}_2\text{O}_3)_x$ ($x = 0.04, 0.08, 0.10, 0.12, \text{ and } 0.14$) solid solutions were grown by directional crystallization of the melt in a cold crucible. It was shown that, in the investigated composition range, homogeneous transparent single crystals were obtained at $x = 0.08\text{--}0.14$ for the $(\text{ZrO}_2)_{1-x}(\text{Y}_2\text{O}_3)_x$ solid solutions and at $x = 0.10\text{--}0.14$ for the $(\text{ZrO}_2)_{1-x}(\text{Gd}_2\text{O}_3)_x$ solid solutions.

It was established that the cubic phase in the crystals co-doped with Y_2O_3 stabilizes at the lower Y_2O_3 concentration in the solid solution than in the crystals co-doped with Gd_2O_3 . This can be attributed to the dependence of stabilization of the high-temperature phase on the stabilizing impurity type.

It was established that the local crystal environment of Eu^{3+} ions in the $(\text{ZrO}_2)_{1-x}(\text{Y}_2\text{O}_3)_x$ and $(\text{ZrO}_2)_{1-x}(\text{Gd}_2\text{O}_3)_x$ solid solutions is determined by the stabilizing oxide concentration and, in this case, almost independent of its type (Y_2O_3 or Gd_2O_3). The maximum conductivity at a temperature of 1173 K was observed in the crystals containing 10 mol % of Gd_2O_3 and 8 mol % of Y_2O_3 . These compositions correspond to the t'' phase and are similar to the interface between the cubic and tetragonal phase regions. The data obtained allow us to conclude that, in the investigated composition range, the concentration dependence of the ionic conductivity is affected mainly by the phase composition rather than the character of the localization of oxygen vacancies in the crystal lattice.

FUNDING

This study was supported by the Russian Science Foundation, project no. 18-79-00323.

REFERENCES

1. *Science and Technology of Zirconia V*, Badwal, S.P.S., Bannister, M.J., and Hannink, R.H.J., Eds., Lancaster: Technomic Pub., 1993.
2. Basu, R.N., Materials for solid oxide fuel cells, in *Recent Trends in Fuel Cell Science and Technology*, New Delhi, India: Anamaya, 2007, chap. 12, pp. 284–329. <https://doi.org/10.1007/978-0-387-68815-2>
3. Yamamoto, O., Arachi, Y., Sakai, H., Takeda, Y., Imanishi, N., Mizutani, Y., Kawai, M., and Nakamura, Y., Zirconia based oxide ion conductors for solid oxide fuel cells, *Ionics*, 1998, vol. 4, nos. 5–6, pp. 403–408. <https://doi.org/10.1007/BF02375884>
4. Kuzminov, Yu.S., Lomonova, E.E., and Osiko, V.V., *Tugoplavkie materialy iz kholodnogo tiglya* (Refractory Materials from a Cold Crucible), Moscow: Nauka, 2004.
5. Arachi, Y., Sakai, H., Yamamoto, O., Takeda, Y., and Imanishi, N., Electrical conductivity of the $\text{ZrO-Ln}_2\text{O}_3$ ($\text{Ln} = \text{lanthanides}$) system, *Solid State Ionics*, 1999, vol. 121, nos. 1–4, pp. 133–139. [https://doi.org/10.1016/S0167-2738\(98\)00540-2](https://doi.org/10.1016/S0167-2738(98)00540-2)

6. Kilner, J.A. and Brook, R.J., A study of oxygen ion conductivity in doped non-stoichiometric oxides, *Solid State Ionics*, 1982, vol. 6, no. 3, pp. 237–252. [https://doi.org/10.1016/0167-2738\(82\)90045-5](https://doi.org/10.1016/0167-2738(82)90045-5)
7. Kilner, J.A. and Waters, C.D., The effects of dopant cation-oxygen vacancy complexes on the anion transport properties of non-stoichiometric fluorite oxides, *Solid State Ionics*, 1982, vol. 6, no. 3, pp. 253–259. [https://doi.org/10.1016/0167-2738\(82\)90046-7](https://doi.org/10.1016/0167-2738(82)90046-7)
8. Goff, J.P., Hayes, W., Hull, S., Hutchings, M.T., and Clausen, K.N., Defect structure of yttria-stabilized zirconia and its influence on the ionic conductivity at elevated temperatures, *Phys. Rev. B*, 1999, vol. 59, no. 22, pp. 14202–14219. <https://doi.org/10.1103/PhysRevB.59.14202>
9. Yugami, H., Koike, A., Ishigame, M., and Suemoto, T., Relationship between local structures and ionic conductivity in ZrO_2 - Y_2O_3 studied by site-selective spectroscopy, *Phys. Rev. B*, 1991, vol. 44, no. 17, pp. 9214–9222. <https://doi.org/10.1103/PhysRevB.44.9214>
10. Catlow, C.R.A., Transport in doped fluorite oxides, *Solid State Ionics*, 1984, vol. 12, pp. 67–73. [https://doi.org/10.1016/0167-2738\(84\)90131-0](https://doi.org/10.1016/0167-2738(84)90131-0)
11. Zavodinsky, V.G., The mechanism of ionic conductivity in stabilized cubic zirconia, *Phys. Solid State*, 2004, vol. 46, no. 3, pp. 453–457. <https://doi.org/10.1134/1.1687859>
12. Tokiy, N.V., Perekrestov, B.I., Savina, D.L., and Danilenko, I.A., Concentration and temperature dependences of the oxygen migration energy in yttrium-stabilized zirconia, *Phys. Solid State*, 2011, vol. 53, pp. 1827–1901. <https://doi.org/10.1134/S1063783411090290>
13. Ding, H., Virkar, A.V., and Liu, F., Defect configuration and phase stability of cubic versus tetragonal yttria-stabilized zirconia, *Solid State Ionics*, 2012, vol. 215, pp. 16–23. <https://doi.org/10.1016/j.ssi.2012.03.014>
14. Li, X. and Hafskjold, B., Molecular dynamics simulations of yttrium-stabilized zirconia, *J. Phys.: Condens. Matter*, 1995, vol. 7, pp. 1255–1271. <https://doi.org/10.1088/0953-8984/7/7/007>
15. Eichler, A., Tetragonal Y-doped zirconia: structure and ion conductivity, *Phys. Rev. B*, 2001, vol. 64, no. 17, pp. 174103-1–174103-8. <https://doi.org/10.1103/PhysRevB.64.174103>
16. Dexpert-Ghys, J., Faucher, M., and Caro, P., Site selective spectroscopy and structural analysis of yttria-doped zirconias, *J. Solid State Chem.*, 1984, vol. 54, no. 2, pp. 179–192. [https://doi.org/10.1016/0022-4596\(84\)90145-2](https://doi.org/10.1016/0022-4596(84)90145-2)
17. Voron'ko, Yu.K., Zufarov, M.A., Sobol', A.A., Ushakov, S.N., and Tsybmal, L.I., Spectroscopy and structure of Eu^{3+} centers in partially stabilized zirconia and hafnia, *Inorg. Mater.*, 1997, vol. 33, no. 4, pp. 379–389.
18. Borik, M.A., Volkova, T.V., Kuritsyna, I.E., Lomonova, E.E., Myzina, V.A., Ryabochkina, P.A., and Tabachkova, N.Yu., Features of the local structure and transport properties of ZrO_2 - Y_2O_3 - Eu_2O_3 solid solutions, *J. Alloys Compd.*, 2019, vol. 770, pp. 320–326. <https://doi.org/10.1016/j.jallcom.2018.08.117>
19. Borik, M.A., Lomonova, E.E., Osiko, V.V., Panov, V.A., Porodinkov, O.E., Vishnyakova, M.A., Voron'ko, Yu.K., and Voronov, V.V., Partially stabilized zirconia single crystals: growth from the melt and investigation of the properties, *J. Cryst Growth*, 2005, vol. 275, nos. 1–2, pp. e2173–e2179. <https://doi.org/10.1016/j.jcrysgro.2004.11.244>
20. Andrievskaya, E.R., *Fazovye ravnovesiya v sistemakh oksidov gafniya, tsirkoniya, itriya s oksidami redkozemel'nykh elementov* (Phase Equilibria in Systems of Oxides of Hafnium, Zirconium, Yttrium with Oxides of Rare-Earth Elements), Kiev: Naukova Dumka, 2010.
21. Yashima, M., Sasaki, S., Kakihana, M., Yamaguchi, Y., Arashi, H., and Yoshimura, M., Oxygen-induced structural change of the tetragonal phase around the tetragonal-cubic phase boundary in ZrO_2 - $YO_{1.5}$ solid solutions, *Acta Crystallogr., B*, 1994, vol. 50, no. 6, pp. 663–672. <https://doi.org/10.1107/S0108768194006257>
22. Judd, B.R., Three-particle operators for equivalent electrons, *Phys. Rev.*, 1966, vol. 141, no. 1, pp. 4–14. <https://doi.org/10.1103/PhysRev.141.4>
23. Krupke, W.F., Optical absorption and fluorescence intensities in several rare-earth-doped Y_2O_3 and LaF_3 single crystals, *Phys. Rev.*, 1966, vol. 145, no. 1, pp. 325–337. <https://doi.org/10.1103/PhysRev.145.325>
24. Bol'shakova, E.V., Malov, A.V., Ryabochkina, P.A., Ushakov, S.N., and Nishchev, K.N., Intensities of hypersensitive transitions in garnet crystals doped with Er^{3+} ions, *Opt. Spectrosc.*, 2011, vol. 110, no. 6, pp. 910–916. <https://doi.org/10.1134/S0030400X11060038>
25. Borik, M.A., Volkova, T.V., Lomonova, E.E., Myzina, V.A., Ryabochkina, P.A., Tabachkova, N.Yu., and Chabushkin, A.N., Spectroscopy of optical centers of Eu^{3+} ions in partially stabilized and stabilized zirconium crystals, *Opt. Spectrosc.*, 2017, vol. 122, no. 4, pp. 580–587. <https://doi.org/10.1134/S0030400X17040087>

Translated by E. Bondareva